Superconductor
Science and
Technology

PAPER • **OPEN ACCESS**

An analytical model for predicting the magnetization loss in HTS sector-shaped conductors for fusion

To cite this article: Gianluca De Marzi *et al* 2024 *Supercond. Sci. Technol.* **37** 125007

OPEN ACCESS
IOP Publishing
Superconductor Science and Technology
Supercond. Sci. Technol. **37** (2024) 125007 (13pp)
https://doi.org/10.1088/1361-6668/ad8af4

An analytical model for predicting the magnetization loss in HTS sector-shaped conductors for fusion

Gianluca De Marzi[1,*], **Luigi Muzzi**[1] and **Francesco Grilli**[2]

[1] ENEA, Nuclear Department, via Enrico Fermi 45, 00044 Frascati, Italy
[2] Karlsruhe Institute of Technology, 76344 Eggenstein-Leopoldshafen, Germany

E-mail: gianluca.demarzi@enea.it

Received 19 June 2024, revised 8 October 2024
Accepted for publication 24 October 2024
Published 6 November 2024

Abstract

Within the framework of magnetic confinement fusion, several projects worldwide are demonstrating the possibility of integrating high-temperature superconductors (HTS) in the coil systems. HTS-based technologies are highly attractive for practical applications because they can extend the operating margins of fusion coils in terms of higher temperatures, transport currents and magnetic fields. Based on the results achieved with the twisted-stacked tape cable, we have designed a novel low-loss HTS sector cable-in-conduit conductor, with a target of 60 kA at 4.5 k, 18 T, which is presently of interest for the DEMO Central Solenoid coil. In HTS cables, the AC losses can represent a significant limiting factor, therefore they must be taken into consideration both in the design phase and in the assessment of the overall magnet thermal budget. In this work, to assess the loss behavior and to optimize the cable design, we have explored different aspect ratios and arrangements of the stacked tapes within the cable layout. The magnetization losses are calculated with a 2D finite-element model based on the T-A formulation and analytical approximations based on the Brandt-Halse critical state model. Specifically, we have developed an analytical formulation that allows for the calculation of the instantaneous power losses in HTS stacked cables with a limited number of tapes per stack, achieving sufficient accuracy at high fields. The analytical model enables a sufficiently accurate assessment of the heat deposited on the conductor during those particular instants of a plasma scenario where the variation of the field is very high, such as during the critical initial discharge period of the plasma initiation.

Keywords: fusion, AC losses, hysteresis loss, HTS cables, numerical modeling, finite-elements

* Author to whom any correspondence should be addressed.

1. Introduction

Nowadays, the rapid development and rising market of high-temperature superconductors (HTS) have spurred the magnet designers to explore their suitability and advantages in the context of fusion research. HTS tokamaks hold significant promise due to their ability to achieve higher magnetic fields, potentially enabling the realization of much smaller machines with shorter construction time [1]. However, the mechanical stresses and heat loads in these compact devices pose formidable challenges.

The EUROfusion Consortium is also contemplating the utilization of HTS-based technology in EU-DEMO, the future European nuclear fusion reactor. Although the implementation of HTS is presently considered economically unfeasible for large-size toroidal field (TF) fusion coils [2], within the EU-DEMO a feasibility study for a TF winding pack option based solely on HTS has been carried out [3]. Conversely, in the case of the central solenoid a hybrid solution has been proposed. This hybrid approach employs HTS, Nb_3Sn, and NbTi conductors for the high, medium and low field sections, respectively [4]. A hybrid design offers a promising advantage for either a reduction in the solenoid's outer radius—which could decrease the overall tokamak size and cost—or an enhancement in the generated magnetic flux, potentially extending the plasma burn duration time [4–6].

Regarding the technologies for the HTS coils, a specific target has been defined with the development of an HTS cable-in-conduit conductor, which should demonstrate effective and stable operation under conditions involving 60 kA current, 18 T magnetic field strength, and a temperature of 4.5 K; the conductor should also be capable of operating in pulsed conditions [7]. In recent research developments at ENEA [7], we have designed a novel concept for HTS sector cables, denoted as the SECtor-ASsembled cable (SECAS) based on BRAided Stacks of Tapes (BRAST). Each BRAST sub-unit comprises a stack of an arbitrary number of tapes assembled within a braid of thin, tin coated Cu wires. This BRAST architecture serves a dual purpose: it facilitates the handling of the tape stack while ensuring its protection throughout the entire cable manufacturing process. Given the current performance capabilities of commercial coated conductors, the target specifications (60 kA, 18 T) can be obtained with six BRASTs, each containing ten 12 mm wide tapes.

Several trials have been carried out, to verify the manufacturing approach, using either Al- or Cu-based stabilizers; figure 1 shows an optical image of the cross-section of a jacketed Cu-stabilized SECAS cable. The copper wires forming the braid are clearly visible around the 10-tape stack. The stack is held in place by a copper filler.

Different configurations for the cross-section in each cable sector have been considered so far [7]: (A) one BRAST made of ten 12 mm-wide tapes; (B) two BRASTs, each made of five 12 mm-wide tapes; (C) six BRASTs, each made of five 4 mm wide tapes. These diverse configurations, shown schematically in figure 2, can impact the AC losses, and need to be studied in detail.

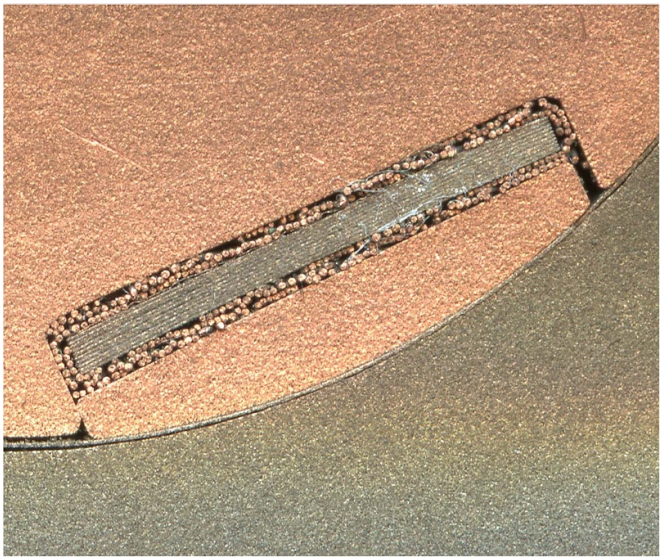

Figure 1. Optical image showing the cross-section of a Cu-stabilized SECAS cable. The stack is housed in a slot, and the braid is clearly visible around the stack. The braided stack is held in place by a copper filler plus the external jacket.

The aim of the present work is to develop an analytical model for the calculation of the instantaneous power losses in a twisted stacked-tape cable (TSTC) with a limited number of tapes in the stacks, in an operational environment typical of a fusion reactor. The main novelty of this work lies in the development of an analytical formulation for calculating the instantaneous power losses in HTS stacked cables with a limited number of tapes per stack, achieving sufficient accuracy at high magnetic fields. This model is valid for any periodic waveform and enables a precise assessment of the heat deposited on the conductor during specific moments of plasma scenarios, such as the critical initial discharge period of plasma initiation, where the field variation is particularly rapid. This method provides a faster alternative to computationally intensive finite-elements (FE) models, offering a robust framework for ballpark AC loss estimations.

Through this work, this analytical methodology will be applied to the three layout configurations defined above, but with the aim of developing a framework of general validity that can be applied to any stacked-tape or conductor-on-round core cable layouts. The knowledge of the time evolution of the hysteretic power loss would also be helpful for detailed studies, e.g. thermal-hydraulic analysis [8], or to determine the power deposited in those time instants of the plasma scenario where the variation of the field is very high, i.e. at the breakdown phase of the plasma start-up [9].

This paper is structured as follows: section 2 outlines the theoretical background for assessing the power dissipation in superconductors. Section 3 details the numerical methods employed for simulating HTS tape stacks with perpendicular or parallel field configurations. Section 4 explores different analytical approaches for calculating AC losses. A modified Brandt solution is proposed for the stack in a

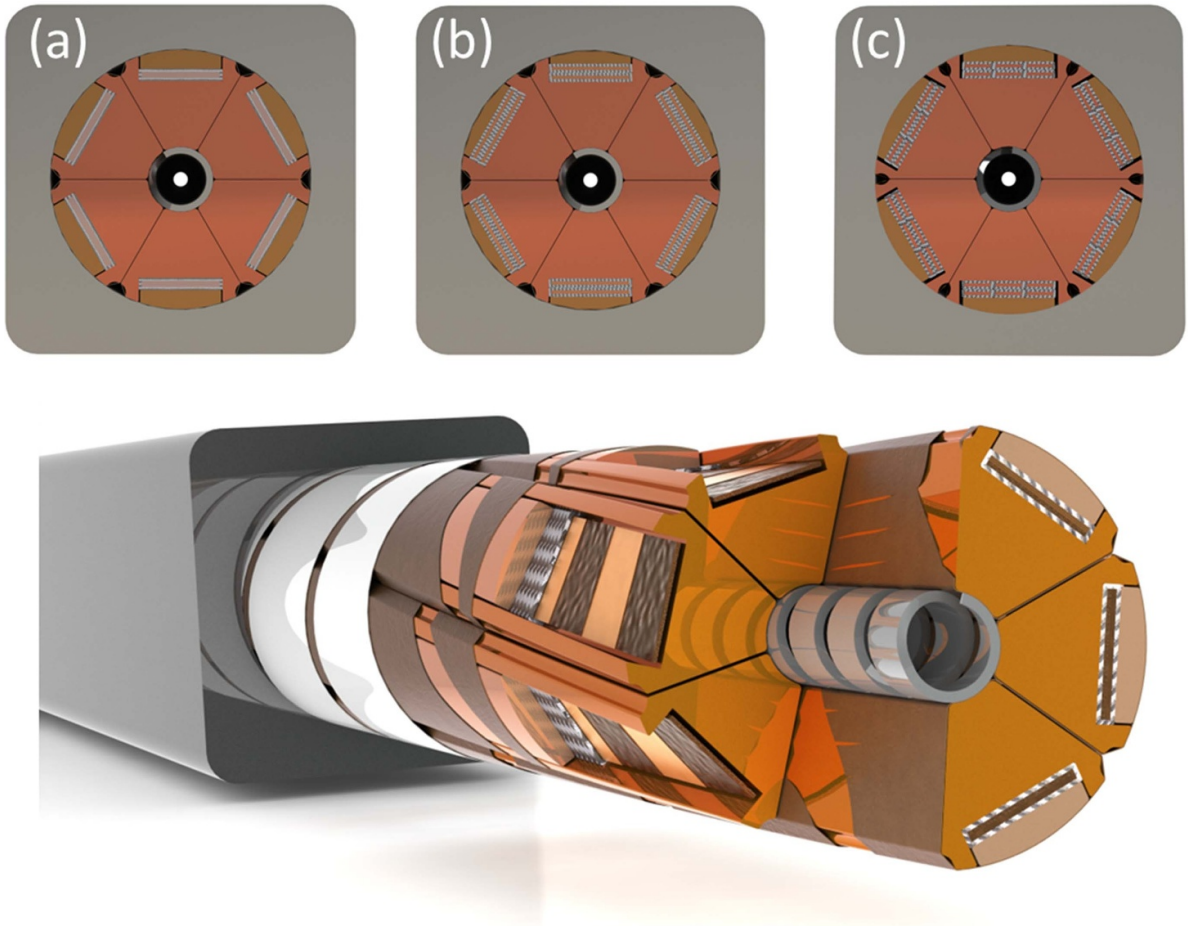

Figure 2. Schematic representation of the three cross-sections of the SECAS HTS Sector Shaped high-current Conductor considered in this work. Each sector contains: (a) one BRAST made of ten 12 mm-wide tapes; (b) two BRASTs, each made of five 12 mm-wide tapes; and (c) six BRASTs, each made of five 4 mm wide tapes. Bottom: perspective representation of the assembled SECAS conductor with BRASTs, sector-shaped core, fillers, outer steel wrap, and central spiral.

perpendicular field. Tilted and twisted configurations are also discussed. Section 5 provides an analysis of the AC losses in sector-shaped high-current conductors, integrating both numerical and analytical approaches. Finally, section 6 wraps up with the conclusions, highlighting the main findings and their practical implications.

2. Local dissipation and AC losses

A quantity of practical relevance in the design of large-scale applications is the power dissipation under varying transport currents and magnetic fields [10].

The power dissipation per unit volume, p, in both superconducting and normal materials, induced by any current density $\mathbf{J}$ in a given electric field $\mathbf{E}$, is described as follows:

$$p = \mathbf{E} \cdot \mathbf{J} \tag{1}$$

where $\mathbf{E}(\mathbf{J})$ is the constitutive relation of the material. For a superconductor, $\mathbf{E}(\mathbf{J})$ is a nonlinear function of $\mathbf{J}$:

$$\mathbf{E}(\mathbf{J}) = \rho(\mathbf{J})\mathbf{J} \tag{2}$$

where the resistivity

$$\rho(\mathbf{J}) = \frac{E_c}{J_c}\left(\frac{|\mathbf{J}|}{J_c}\right)^{n-1} \tag{3}$$

is a scalar function of $\mathbf{J}$, n being an index defining the steepness of the transition from the superconducting to the normal state, and J_c the critical current density determined by an electric field criterion E_c.

This expression, valid for most hard superconductors for $|\mathbf{J}|$ close to J_c, is the most commonly used relation for superconductor modelling. In the limit of $n \to \infty$, the power law relation in (3) corresponds to the critical state model (CSM), also known as Bean's model [11] in which [10]:

$$|\mathbf{J}|(|\mathbf{E}|) = \begin{cases} J_c & |\mathbf{E}| > 0, \\ \text{any } |\mathbf{J}| \text{ with } |\mathbf{J}| \leqslant J_c & |\mathbf{E}| = 0. \end{cases} \tag{4}$$

From (1), the total instantaneous power loss, P, in the sample is

$$P = \int_v \mathrm{d}^3 r\, p = \int_v \mathrm{d}^3 r\, \mathbf{E}\cdot\mathbf{J} \tag{5}$$

where v denotes the volume of the superconducting fraction of the sample within which the power loss is being calculated, whereas the loss per cycle for periodic excitation (applied magnetic field or current) is given by:

$$Q = \int_0^T \mathrm{d}t \int_v \mathrm{d}^3 r\, \mathbf{E}\cdot\mathbf{J} \tag{6}$$

where T is the period of the periodic excitation.

Both J_c and the transition index n depend on $|\mathbf{B}|$ and the orientation of the magnetic field relative to the superconductor crystallographic axes.

For the description of the magneto-angular dependence of the in-field critical current of commercial 2G-HTS tapes, $J_c(|\mathbf{B}|,\theta)$, we consider an extended version of the conventional Kim model [12], which has been developed by Zhang *et al* [13] by taking into account Blatter's angular anisotropy parameter [14], $\epsilon(\theta)$, as follows:

$$I_c(|\mathbf{B}|,\theta) = \frac{I_{c0}}{\left[1+\epsilon(\theta)\left(\frac{|\mathbf{B}|}{B_0}\right)^{\alpha}\right]^{\beta}} \tag{7}$$

with

$$\epsilon(\theta) = \sqrt{\gamma^{-2}\sin^2(\theta)+\cos^2(\theta)}. \tag{8}$$

In (7), I_{c0}, B_0, α and β are empirical parameters dependent on the specific coated conductor tape; in (8), $\gamma^{-2} = m_{ab}/m_c$ is the anisotropy ratio [14], with m_{ab} and m_c being the effective masses along the *ab*-plane and the *c*-axis, respectively, whereas θ is the angle between the applied field and the *c*-axis.

Experimental data of 12 mm-wide I_c of commercial tapes at low temperatures (< 5 K) and high fields (> 10 T) are scarcely available in the literature, particularly when the field is parallel to the flat surface of the tapes. In this study, we have reconstructed the field-dependence of I_c in both parallel and perpendicular field configurations by appropriate scaling of the available experimental data under slightly different *B*-*T* conditions, see figure 3 [15]. The best fits of (7) to the curves of figure 3 have been obtained with a non-linear least-squares minimization method. With the anisotropy ratio fixed at $\gamma = 5$, as expected in tapes with weak correlated pinning [16, 17], the obtained fitting parameters are as follows: $I_{c0} = 12.2\text{kA}, \alpha = 0.54, \beta = 2.18$, and $B_0 = 5.72\text{T}$.

In the subsequent sections of the paper, we will exclusively focus on hysteresis losses, i.e. the power losses resulting from superconducting currents which form closed loops solely within the superconducting domains. Furthermore, in the following we will only consider an external field varying sinusoidally over time, in the absence of transport current in the conductor.

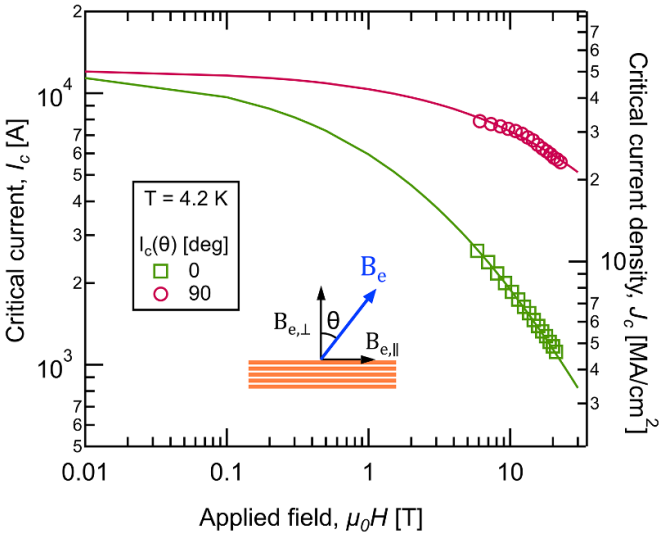

Figure 3. In-field dependence of the critical current, I_c, in parallel and perpendicular field. The experimental data, represented by markers, have been extracted from the data-bank provided by Shanghai Superconductor Technology [15]). The curves have been reconstructed through the scaling the experimental data obtained from 4 mm-wide tapes at temperatures of 4.2 K ($\theta = 0$deg) and 20 K ($\theta = 90$deg), where θ represents the angle between the external field, B_e, and the *c*-axis, as illustrated in the inset. The critical current density, J_c, has been estimated by assuming a thickness of 2 μm for the superconducting layer. Continuous lines represent the best fits curves obtained using the parameters in (7): $I_{c0} = 12.2\text{kA}, \alpha = 0.54, \beta = 2.18$, and $B_0 = 5.72\text{T}$.

3. Numerical methods

In this section, we detail the ground of the numerical methods that we have applied to the modelling of stacks of HTS tapes, by considering for simplicity only FE models implemented in the commercial software COMSOL Multiphysics [18].

3.1. T-A formulation

The T-A formulation is an efficient approach to simulate infinitely thin superconductors [19, 20], which approximate the superconducting layer of HTS coated conductors.

In this formulation, the Faraday's equation is written as:

$$\nabla\times\rho\nabla\times\mathbf{T} = -\partial_t\nabla\times\mathbf{A} \tag{9}$$

where $\mathbf{A}$ is the magnetic vector potential used to calculate the magnetic field in all the simulated domains, whereas $\mathbf{T}$ is the current vector potential:

$$\nabla\times\mathbf{T} = \mathbf{J}. \tag{10}$$

While the surrounding non-conducting medium is modelled as a material with high resistivity in accordance with linear Ohm's law, typically of the order of 1 Ωm, the superconducting layers are modelled using the nonlinear resistivity given by (3).

In this work, a 2D planar geometry is assumed, therefore the thin superconducting layers can be modelled as 1D strips. A schematic of the 2D T-A physical model, along with the

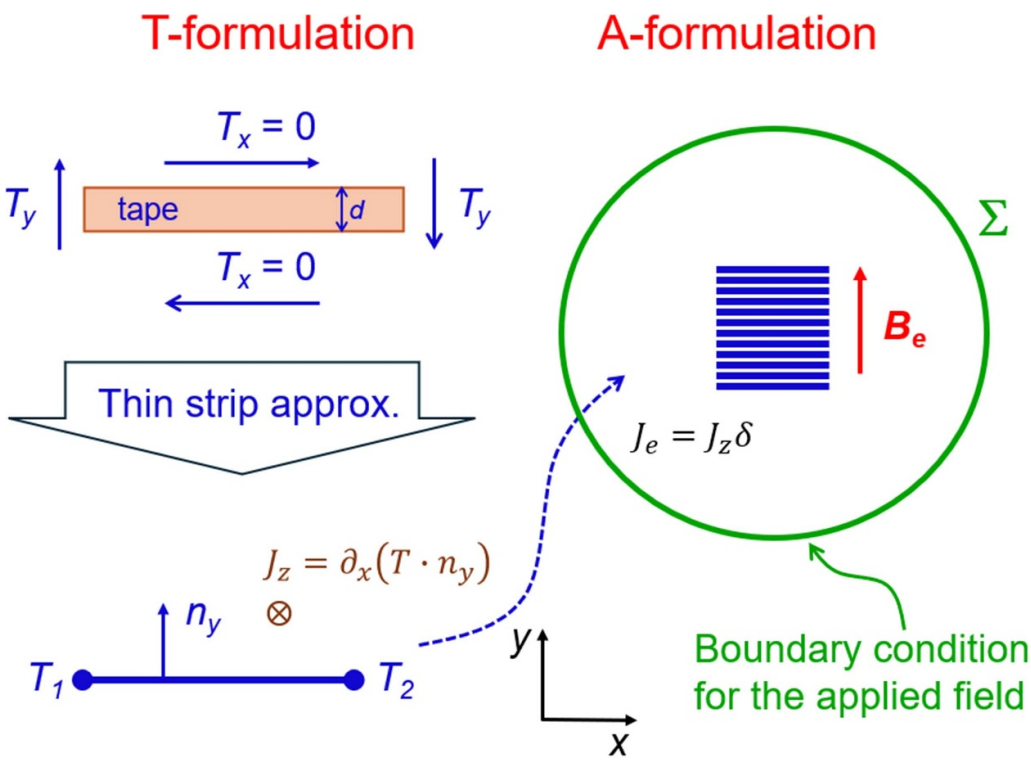

Figure 4. Schematic representation of the 2D T-A model and the coordinate system used for modeling a superconducting stack subjected to an external field oriented perpendicularly to the flat surface of the tapes. The current vector potential **T** is evaluated only in the superconducting strips, whereas the vector potential **A** is computed everywhere. The screening currents are enforced by boundary conditions at the edges T_1 and T_2 of the tape ($T_1 = T_2 = 0$).

stack geometry and the coordinate system, is shown in figure 4. Since the strips are infinitely thin and infinitely long in the z-direction, the current can only flow in the longitudinal direction, the current vector potential being always parallel to the normal vector of the superconducting strip at each point [19].

Therefore, if for example the strips lie in the x-direction, (9) and (10) can be simplified as follows:

$$\partial_x \rho \left(\partial_x \mathbf{T} \cdot n_y\right) = -\partial_t \partial_x A_z \tag{11}$$

$$J_z = \partial_x \left(\mathbf{T} \cdot n_y\right). \tag{12}$$

The external field can be applied by imposing a Dirichlet boundary condition on the outer boundary of the air domain of the type:

$$\begin{cases} B_x = f_x(t) \\ B_y = f_y(t). \end{cases} \tag{13}$$

In (13), B_x and B_y represent the two components of the magnetic flux induction, while $f_x(t)$ and $f_y(t)$ describe the variation of the applied external field over time.

In the present study, we assume that the external field varies sinusoidally as $B_e = B_{em}\sin(\omega t)$ along the y-direction, where B_{em} is the maximum field and ω the angular frequency.

As a concluding remark for this section, the T-A formulation considers only the screening currents within the superconducting layers and does not account for coupling currents between the 1D strips. This approach assumes electrical insulation between the strips and focuses on estimating AC losses due to screening currents. It is important to acknowledge that coupling currents, which could introduce additional losses, are not included in this model. While this simplification offers a useful approximation for the purposes of our study, it is worth noting that it may not fully capture the complete AC loss spectrum in practical applications.

3.2. 1-D diffusion-like model for the Bean slab

Considering the right-handed Cartesian coordinate system centered in the Bean slab (of infinite height z, depth y, and width d; see figure 5), Faraday's equation takes the form:

$$\partial_x E_y(x,t) = -\partial_t B_z(x,t) \tag{14}$$

while the Ampére's law can be written as:

$$\partial_x B_z(x,t) = -\mu_0 J_y(x,t). \tag{15}$$

The combination of (14), (15), and the power law (2) law leads to the following scalar diffusion-like equation [21]:

$$\partial_t B_z(x,t) - \partial_x \left[\frac{\rho}{\mu_0}\partial_x B_z(x,t)\right] = 0. \tag{16}$$

The external field is applied through the following boundary condition for B_z:

$$B_z\left(|x| = \frac{d}{2}, t\right) = B_{em}\sin(\omega t) \tag{17}$$

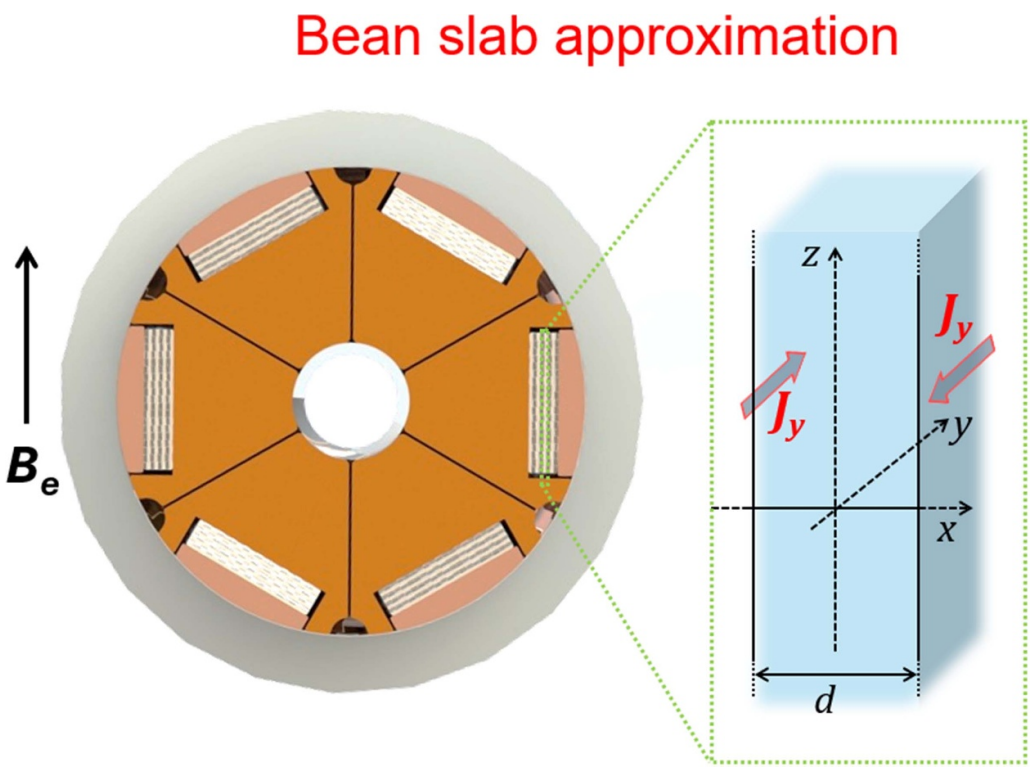

Figure 5. Schematic representation of the 1D Bean's slab model and the coordinate system used for modeling a superconducting stack subjected to an external field parallel to the flat surface of the tapes. Each tape is represented by an infinite slab of thickness δ oriented in the y, z-plane with an externally applied magnetic field B_e directed along z direction. The induced shielding current density J_y flowing in the y direction inside the front and back faces is shown.

where t is time; d is the thickness of the superconducting layer; x the spatial coordinate ($|x| \leqslant d$); ρ the resistivity of the superconducting slab; and $B_z(x,t)$ is the field profile along the x direction at time t. Once the magnetic field distribution is determined, the current density distribution is obtained by means of (15).

A schematic of the 1D Bean's infinite slab model is shown in figure 5.

4. Analytical methods

Several analytical models for calculating AC losses in superconductors are available in the literature. The reader can find a comprehensive review of analytical models in [22]. Referring only to magnetization losses, among the most used models we recall the theoretical expressions by Halse and Brandt [23, 24] and by London [25] for a tape subjected to a variable field perpendicular or parallel to the tape's flat surface, respectively.

4.1. Formulas for instantaneous power dissipation

4.1.1. Bean's slab. The analytical expressions for the instantaneous AC loss power per unit volume for an infinite slab have been obtained by Kajikawa *et al* [26, 27]. The Kajikawa's equations are valid during the first ramp up, when both the external magnetic field, B_e, and the transport current, I_t are monotonically increased. Macchiagodena *et al* [21] extended the analytical formulation to the more general case in which both B_e and I_t are periodic functions, in-phase with each other. In the absence of transport current, the analytical expressions for the AC loss power during the first energization from the virgin state (no trapped field at the ramp start up) are the following:

$$P_{\text{slab}} = \frac{B_p^2}{2\mu_0}\partial_t B_e \begin{cases} \frac{B_e^2}{B_p^3} & B_e \leqslant B_p \\ \frac{1}{B_p} & B_e \geqslant B_p \end{cases} \tag{18}$$

where $\partial_t B_e$ represents the time derivative of the external field B_e, whereas $B_p = \mu_0 J_c \frac{d}{2}$ is the full penetration field for a single tape. After reaching the peak, the set of equations to be used is:

$$P_{\text{slab}} = \frac{B_p^2}{2\mu_0}|\partial_t B_e| \begin{cases} \frac{(B_m+\text{sgn}(\partial_t B_e)B_e)^2}{4B_p^3} & \text{sgn}(\partial_t B_e)\, B_e \leqslant 2B_p - B_m \\ \frac{1}{B_p} & \text{sgn}(\partial_t B_e)\, B_e \geqslant 2B_p - B_m \end{cases}. \tag{19}$$

To obtain results universally applicable, irrespective of J_c, physical dimensions, and frequency, it is advantageous to normalize the AC loss by employing the following dimensionless quantity:

$$p_{\text{slab}} = \frac{2\mu_0}{B_{p0}}\frac{1}{|\partial_t B_e|_{\text{av}}} P_{\text{slab}} \tag{20}$$

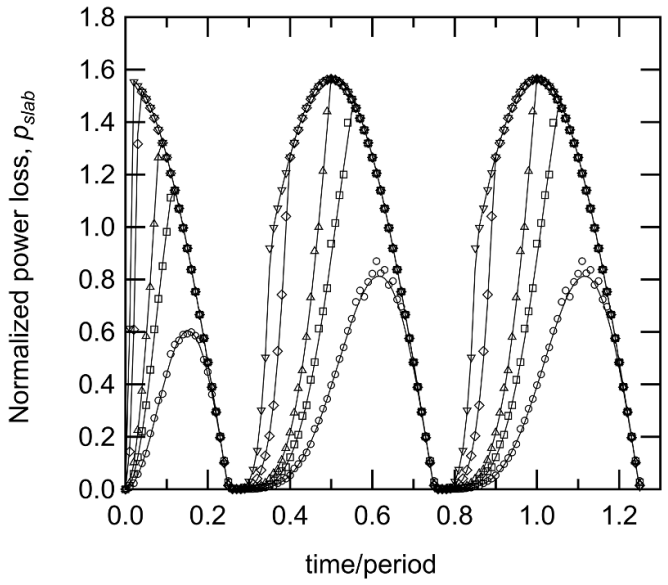

Figure 6. The normalized power loss as a function of time for a 10-tape stack (continuous line), calculated using (20) with a constant J_{c0} and with $|\partial_t B_e|_{av} = 4fB_{em}$ for the sinusoidal field waveform, $B_e(t) = B_{em}\sin(2\pi ft)$. The empty markers represent FE simulations carried out at different values of B_{em}/B_p ratios: 1 (circles); 1.5 (squares); 2 (up-pointing triangles); 5 (diamonds); and 10 (down-pointing triangles).

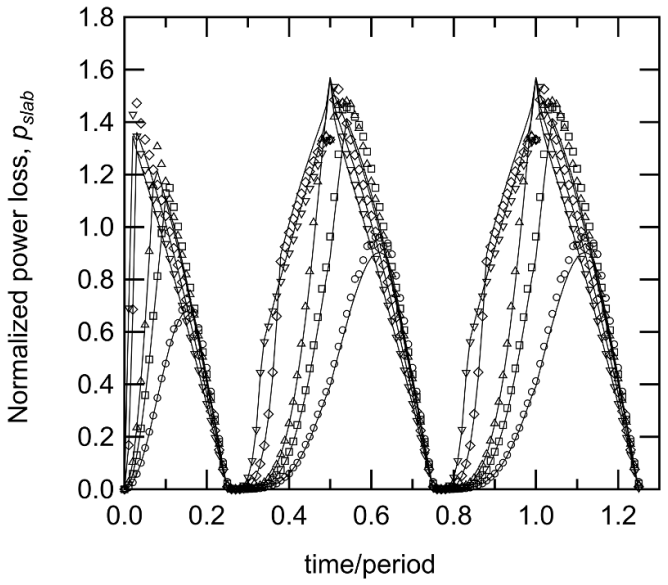

Figure 7. The normalized power loss as a function of time for a 10-tape stack (continuous line), calculated using (20) with a field-dependent J_c and with $|\partial_t B_e|_{av} = 4fB_{em}$ for the sinusoidal field waveform, $B_e(t) = B_{em}\sin(2\pi ft)$. The empty markers represent FE simulations carried out at different values of B_{em}/B_p ratios: 1 (circles); 1.5 (squares); 2 (up-pointing triangles); 5 (diamonds); and 10 (down-pointing triangles).

where B_{p0} is the penetration field at t = 0, and $|\partial_t B_e|_{av}$ is the average of the modulus of $\partial_t B_e$ in a full cycle. For sinusoidal fields, $B_e(t) = B_{em}\sin(2\pi ft)$, the average $|\partial_t B_e|$ is $|\partial_t B_e|_{av} = 4fB_{em}$.

To validate the outcome of the analytical formulae, the time-dependent AC loss has been assessed for a 10-tape stack subjected to a sinusoidally varying field up to $B_{em} = 10B_{p0}$, by considering either a constant J_{c0} or a field-dependent $J_c(B)$.

In both scenarios, the normalized power loss exhibits a peak at each half-cycle and vanishes at the peak of the applied field, as can be seen in figures 6 and 7. In the case of a constant J_{c0}, the agreement between numerical and analytical modeling is excellent, see figure 6. When the critical current J_c depends on the external field, the agreement is not optimal, yet remains more than satisfactory (figure 7). In this latter case, strictly speaking (19) loses its validity as the electric field profiles assume more complex shapes. However, we have verified that at sufficiently high fields (i.e. $\dfrac{B_{em}}{B_{p0}} > 1$), it is still safe to use the analytical Bean's formulas.

4.1.2. Halse-Brandt formula. The analytical expressions for the instantaneous AC loss power per unit volume for an infinitely thin strip have been derived by Brandt [28]:

$$P_{strip} = \frac{1}{4}J_c w|\partial_t B_e|\left[\tanh\left(\frac{B_e}{B_c}\right) - \frac{B_e}{B_c}\mathrm{sech}^2\left(\frac{B_e}{B_c}\right)\right] \quad (21)$$

where $B_c = \mu_0 J_c d/\pi$ and w is the width of the thin strip. Equation (21) is valid for the first magnetization curve, when the field, starting from the virgin state, reaches a maximum value B_{em}. When the applied field B_e oscillates between the extreme values $\pm B_{em}$, the new penetration width $b = d/2\cosh\left[\left(B_{em} + \mathrm{sgn}\left(\partial_t B_e\right)B_e\right)/\left(2B_c\right)\right]$ can be used to obtain a generalized expression for the instantaneous loss:

$$P_{strip} = \tfrac{1}{4}J_c w|\partial_t B_e|\left[\tanh\left(\xi\right) - \xi\,\mathrm{sech}^2\left(\xi\right)\right]$$
$$\xi = \frac{B_{em} + \mathrm{sgn}\left(\partial_t B_e\right)B_e}{2B_c}. \quad (22)$$

It is important to emphasize that this last expression, as well those for the slab, remains valid even if the waveform is not sinusoidal. The integration of (22) over one period yields the well-known Brandt–Halse formula [24]:

$$Q_{loss}\left[\mathrm{Jm}^{-3}\right] = \oint M(H)\,\mathrm{d}H = wJ_c B_c\left[2\ln\cosh\left(\frac{B_{em}}{B_c}\right) - \frac{B_{em}}{B_c}\tanh\left(\frac{B_{em}}{B_c}\right)\right]. \quad (23)$$

Also in this case, it is convenient to use a normalized expression for the instantaneous power loss:

$$p_{strip} = \frac{4}{J_c w}\frac{1}{|\partial_t B_e|_{av}}P_{strip}. \quad (24)$$

As done in the previous sub-paragraph, to validate the analytical formulae, we evaluated the time-dependent AC losses for an infinitely thin strip subjected to a sinusoidally varying field up to $B_{em} = 50B_c$, by considering either a constant J_{c0} or a field-dependent $J_c(B)$. The results are depicted in figures 8 and 9.

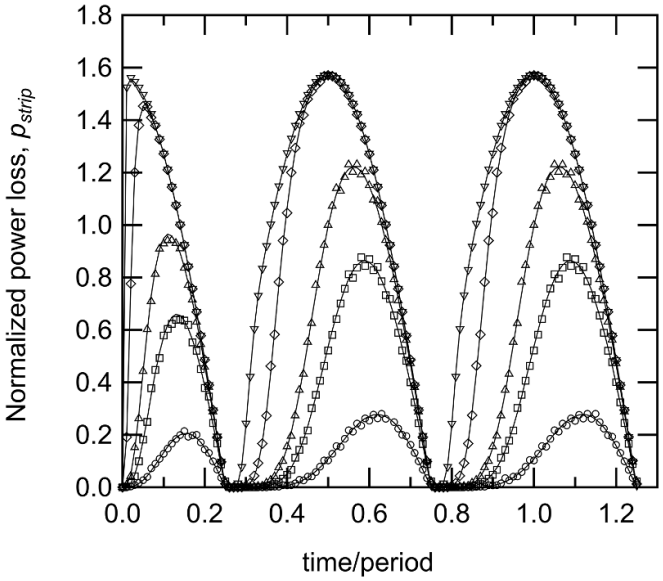

Figure 8. The normalized power loss as a function of time for an infinitely thin strip (continuous line), calculated using (24) with a constant J_{c0} and with $|\partial_t B_e|_{av} = 4fB_{em}$ for the sinusoidal field waveform, $B_e(t) = B_{em}\sin(2\pi ft)$. The empty markers represent FE simulations carried out at different values of B_{em}/B_c ratios: 1 (circles); 2 (squares); 3 (up-pointing triangles); 10 (diamonds); and 50 (down-pointing triangles).

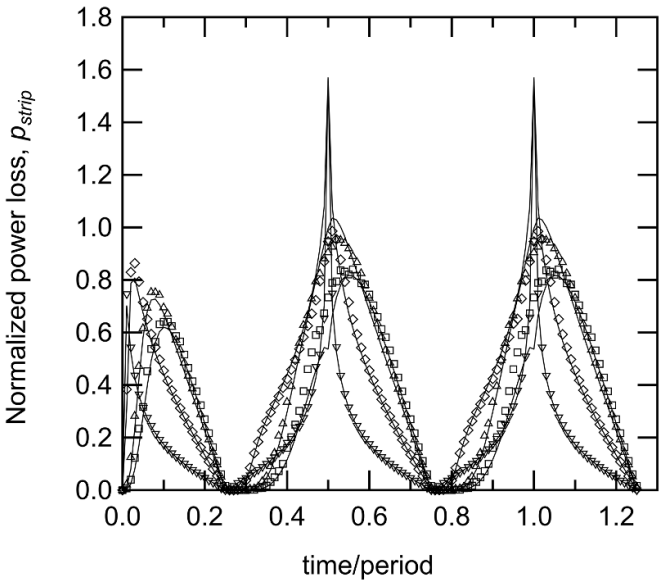

Figure 9. The normalized power loss as a function of time for an infinitely thin strip (continuous line), calculated using (24) with a field-dependent J_c and with $|\partial_t B_e|_{av} = 4fB_{em}$ for the sinusoidal field waveform, $B_e(t) = B_{em}\sin(2\pi ft)$. The empty markers represent FE simulations carried out at different values of B_{em}/B_c ratios: 2 (squares); 3 (up-pointing triangles); 10 (diamonds); and 50 (down-pointing triangles).

Equation (22) has been obtained integrating (1) using the following expression for the electric field [28]:

$$E_x = -\partial_t B_e \left(x^2 - x_p^2\right)^{\frac{1}{2}} \mathrm{sgn}\,(x) \tag{25}$$

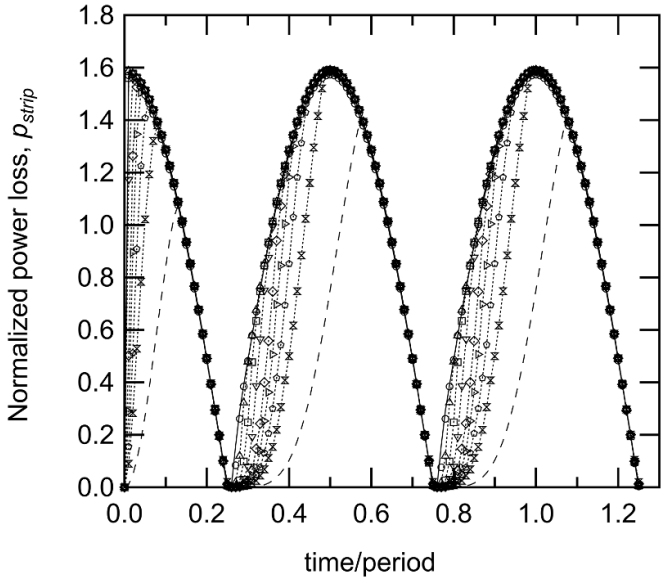

Figure 10. The normalized power loss as a function of time for a N-tape stack, calculated using (24) with a constant J_{c0} and with $|\partial_t B_e|_{av} = 4fB_{em}$ for the sinusoidal field waveform, $B_e(t) = B_{em}\sin(2\pi ft)$, $B_{em} = 18T$. The empty markers represent FE simulations (T-A formulation) carried out for stacks with different number of tapes: $N = 1$ (circles); $N = 2$ (up-pointing triangles); $N = 5$ (squares); $N = 10$ (down-pointing triangles); $N = 20$ (diamonds); $N = 30$ (right-pointing triangles); $N = 50$ (pentagons); and $N = 100$ (hourglasses). The continuous line represents the Brandt–Halse solution for a single strip, whereas the dashed line represents an infinite number of stacked tapes, calculated analytically using the homogeneized Bean slab. Dotted lines are guides to the eye.

where x_p represents the point at which the electric field profile within the strip becomes zero.

However, when a field-dependent $J_c(B)$ is considered, (22) is no longer valid, since the electric field profiles cannot be anymore descibed by (25). Then, we have verified that (22) can be used at sufficiently high fields (i.e. $\frac{B_{em}}{B_c} > 2$), see figure 9.

We now discuss the case of a N-tape stack subjected to a perpendicular field. There exist two distinct limit cases within the CSM where the magnetization of stacks subjected to a perpendicular magnetic field is analytically solved: the Brandt's solution for the single tape, and the Mawatari's solution for a stack with infinite number of tapes [29]. All other cases with a finite number of tapes typically require numerical methods for resolution. If the number of tapes is small nonetheless, it is possible to apply approximations, as we will see at the end of this subsection.

The time-dependent AC loss has been assessed using the T-A formulation for N-tape stacks ($1 \leqslant N \leqslant 100$) exposed to a sinusoidally varying field up to 18 T. The results of the simulations for the various values of N are depicted in figure 10. The curves clearly show a gradual decrease in the normalized power loss with increasing N, indicative of the magnetic shielding effect within the stack (see also [30, 31]). All curves calculated for finite N values lie between the two analytically solved limit cases, as expected.

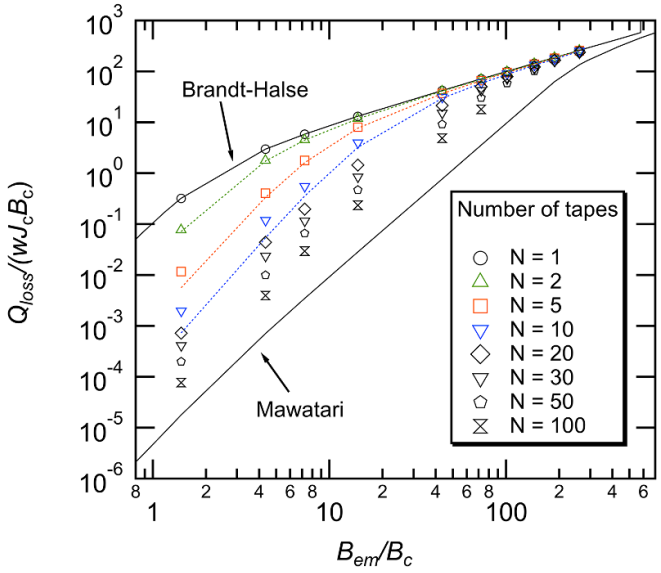

Figure 11. The normalized AC loss as a function of normalized applied field for N-tape stacks. The FE results are represented by empty markers; the continuous line represents the Brandt–Halse limit, whereas the dashed line is the Mawatari limit. Dotted lines represents the approximated solutions obtained analytically by integration of (24) over a full cycle, using $B_c = \mu_0 J_c d N/\pi$.

Figure 11 depicts the numerically evaluated total losses per cycle as a function of the number of tapes in the stack. For the sake of clarity, figure 11 also includes the analytically computed losses in the Brandt–Halse limit (a single tape) and the Mawatari limit (stack with an infinite number of tapes).

As previously noted, there is no analytical solution to the N-tape stack problem. Nonetheless, for a small number of tapes ($N \leqslant 10$), approximations can be made. We have employed the following approach: treating the stack as a single tape, while still employing (24), with adjusting $B_c = \mu_0 J_{c0} N/\pi$. The curves obtained in this manner are depicted as dashed lines in figure 11. It can be observed that such an approach provides a reasonably accurate data representation for stacks with fewer than 10 tapes.

4.2. Tilted stacks

In the literature, a number of studies have investigated the hysteresis losses in tilted stacks [8, 21, 27, 32]. The commonly accepted approach is to separately consider the contributions to AC losses arising from the perpendicular and parallel components of the field, and then simply sum these contributions to obtain the total losses at an arbitrary angle.

In those models, the reference is solely the Bean slab, in which the width D of the infinite slab, the critical current density, $J_{c,slab}$ and the external field B_e are set differently depending on the component being calculated. For the estimation of the parallel-field loss, calculated using (20) ($P_{\parallel} = P_{slab}$), the slab parameters are set to $D = d$, $J_{c,slab} = J_c$, and $B_e = B_{\parallel}$; for the estimation of the perpendicular-field loss, ($P_{\perp} = P_{slab}/\lambda$), the slab parameters are set to $D = w$, $J_{c,slab} = \lambda J_c$, and $B_e = B_{\perp}$ [27]. Here, $\lambda = d/g$, where d is thickness of the superconducting layer within the HTS tape, and g is thickness of the tape). The total AC loss in the stack is then obtained by summing up $P_{\parallel} + P_{\perp}$. However, it is important to consider that the perpendicular-field losses are significantly larger than those due to the parallel-field component. It can be easily verified that, in the high-field limit, equations (19) and (22), assume the following expressions:

$$\lim_{\theta \to \frac{\pi}{2}} P_{slab} = \frac{1}{4} d J_c |\sin(\theta)\, \partial_t B_e| \tag{26}$$

$$\lim_{\theta \to \frac{\pi}{2}} P_{strip} = \frac{1}{4} w J_c |\cos(\theta)\, \partial_t B_e|. \tag{27}$$

Therefore, the two contributions have equal weight when $\theta = \mathrm{atan}(\frac{w}{d}) = 89.99°$. Beyond this value, the losses due to the parallel component dominate over the contribution from the perpendicular component.

Based on these considerations, we determine that employing the T-A formulation is a safe choice. In fact, this formulation is based on the thin strip approximation, which constrains the current to flow only in the plane parallel to the flat face of the tape, thus enabling the reduction of the current vector potential to a scalar quantity. As a result, this formulation of the Maxwell equations inherently neglects any contribution from the parallel-field loss [20, 33]; however, unless the stack is aligned at an angle of $\pi/2$, the parallel component can be safely neglected.

4.3. Twisted stacks

When the stacks are twisted inside the cable, they are subjected to magnetic fields spanning 360° of orientation along one twist pitch length. The instantaneous power loss density of a twisted stack, $P_{twisted}$, is determined as the average value over one twist pitch, obtained by integrating the sum of the two components (19) and (22) arising from perpendicular and parallel fields [34]:

$$P_{twisted} = \frac{2}{\pi} \int_0^{\pi/2} \left[P_{slab}\left(B_{e\parallel}\right) + P_{strip}\left(B_{e\perp}\right) \right] \mathrm{d}\theta \tag{28}$$

where $B_{e\parallel}$ and $B_{e\parallel}$ are the parallel and perpendicular component of the external field, respectively.

At high fields, the power loss can be determined analytically using single-tape models. Specifically, it has been demonstrated [34] that the hysteresis loss of a twisted tape is approximately $2/\pi$ times the hysteresis loss of a single tape in a perpendicular field, if the critical current does not depend on magnetic field.

As a final remark for this section, the analytical approach presented in our study provides a simplified yet effective method for estimating AC losses in superconducting conductors. Despite its assumptions of infinite dimensions and unidirectional current distribution, it yields qualitatively accurate results similar to those obtained from the FE model. Although this manuscript does not include direct comparisons with experimental data, prior validation of the FE model, as cited in

[10], supports the reliability of our approach. Given the strong agreement between the FE and analytical results, we conclude that the analytical method offers a useful, albeit rough, estimation of AC losses in complex conductor configurations. This approach is particularly valuable when experimental data or extensive numerical simulations are not available, providing meaningful insights with minimal computational effort.

5. AC losses of sector-shaped high current conductors

As detailed in the introduction, three configurations for the SECAS cross-section in each cable sector are considered: (A) one BRAST consisting of ten 12 mm-wide tapes; (B) two BRASTs, each composed of five 12 mm-wide tapes; and (C) six BRASTs, each comprising five 4 mm wide tapes. Option-A achieves the target current with the fewest number of tapes; however, due to the wide tapes, AC losses may be higher compared to other solutions. Option-B, although not effective for reducing losses, especially at low fields, is considered because the strain distribution on the tapes belonging to each stack is expected to be narrower. Finally, Option-C is considered because narrower tapes, in accordance with (23), should generate lower AC losses. In this paragraph, we will examine the three options in detail from both numerical and analytical perspectives.

In the 2D FE model, the losses, $P_{\text{loss}}^{\text{FEM}}(\theta)$, can be calculated at a given angleG θ between the stacks and the external field. This FE model incorporates only the 2D T-A formulation, as the losses due to the parallel component are negligible if the angle between the external field and the normal to the wide surface of the stacks is less than 89.99°, as shown in section 4.2. In support of this assumption, we note that in the SECAS cable considered in this section, there will always be at least four stacks that are not aligned parallel to the external field. To address the 3D twisted geometry [8], and considering the 6-fold symmetry of the stacked cable, the simulation can be performed at different orientations of the cable spanning a $\Delta\theta = \pi/3$ range, with the results averaged as follows:

$$P_{\text{loss}}^{\text{FEM}} = \sum_{j=1}^{N_s} P_{\text{loss}}^{\text{FEM}}\left(j\frac{\pi}{3}\frac{1}{N_s}\right) \tag{29}$$

in which N_s is the number of sections. Considering the computational burden of the calculations, it is necessary to keep N_s sufficiently small while still maintaining reasonable convergence, which is already achieved for $N_s = 11$.

We now aim to estimate the instantaneous power losses over one cycle for the three options, considering a sinusoidal variation of the external magnetic field. Using the properties of the tape shown in figure 3, B_c is approximately equal to 0.4 T. Large-scale applications operate at currents or magnetic fields with characteristic frequencies ranging from mHz or below, such as in fusion magnets. Therefore, we have chosen a magnetic field amplitude of $\pm\, 50B_c$ (slightly over 20 T), and a frequency of 1 mHz.

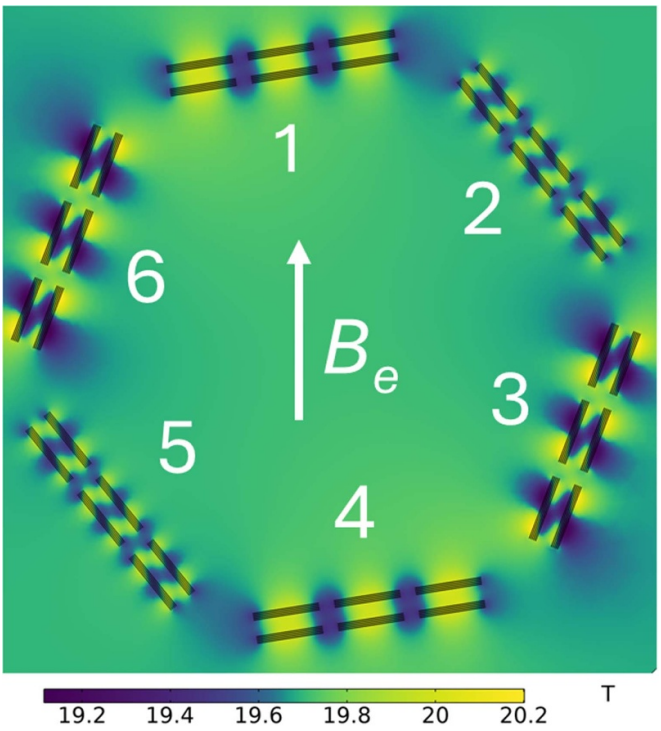

Figure 12. Magnetic field distribution in the Option-C cable, calculated at $T = 4.2$ K at time instant $t/T = 0.29$.

Figure 12 represents the magnetic field distributions at 4.2 K for the Option-C cable at the time $t/T = 0.29$, a few instants after the applied magnetic flux density has reached its maximum. The self-field adds to the background field, thus generating a local non-uniformity with a maximum field of 20.2 T and a minimum field of 19.1 T. In figure 12, the sectors are numbered from 1 to 6, starting at the top and proceeding clockwise. The perpendicular component of the external field varies across the sector pairs 1–4, 2–5, and 3–6, resulting in different J_c values for each case. This variation is reflected in the local magnetic field configuration, as clearly illustrated in the figure.

Figure 13 shows the instantaneous power loss, expressed in W/m, as a function of time for all three cable options considered. The numerical simulations are calculated using (29) and are represented by markers, while solid lines represent the analytically calculated curves using (28).

The integration of the numerical curve for cable Option-A yields 23.9 kJ m^{-1} (per cycle), whereas the analytical formula provides a value approximately 14% higher, namely 27.1 kJ m^{-1} (per cycle).

The comparison between the integrated AC losses obtained throughout the numerical model and the analytical formulation can be considered overall good. It is important to note the following points: (1) the approximations adopted for the stack, where B_c in (22) is approximated as $B_c = \mu_0 J_{c0} dN/\pi$; (2) the T-A formulation does not account for the field components parallel to the tapes; and (3) the analytical formulas do not consider that the magnetic field at the stack edges can

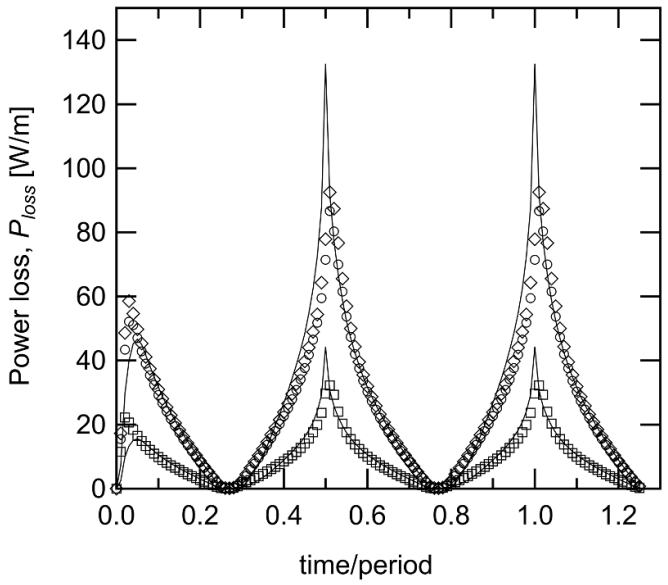

Figure 13. The instantaneous power loss as a function of time for the three options of the SECAS cable. The markers represent the numerical results: Option-A (circles); Option-B (diamonds); and Option-C (squares). The analytical calculations, obtained using (28), are plotted as continuous lines.

differ from the background field. Based on these considerations, it can be asserted that the agreement between the FEM model and the analytical formulation is more than satisfactory.

The analytical calculation of losses in Option-B is more complex due to the high local magnetic field and the reduced distance between the 5-tape stacks within the same sector, whose magnetic interaction cannot be ignored. Specifically, separating the 10-tape stack into two subgroups reduces the stacking effect previously discussed in figure 11, consequently increasing the losses. The integration of the numerical curve for cable Option-B yields 25.4 kJ m^{-1} (per cycle), 6.5% higher than Option-A. As expected, the analytical equations fail to provide a consistent value for the Option-B cable: using $N = 5$ tapes in (28) results in an integrated loss of 30.9 kJ m^{-1} (per cycle), 21% higher than the FEM results.

The Option-C cable exploits the loss-reducing strategy extensively documented in the literature [35, 36], namely, the use of a thin conductor in the direction perpendicular to the field. As evident from (22), the hysteretic loss is proportional to the width of the conductor. Therefore, by modifying the aspect ratio of the conductor, it is possible to control the loss. The aspect ratio can be adjusted by substituting the 12 mm tape stacks with stacks of narrower tapes. This strategy is highly effective in reducing losses. For the Option-C cable, numerical simulations show an integrated power per cycle of 8.8 kJ m^{-1} (per cycle), which represents 37% of the loss assessed for the Option-A cable, a value close to the expected 1/3. The analytical approach also aligns with the expected reduction due to the aspect-ratio modification: the estimated losses are 9.0 kJ m^{-1} (per cycle).

In summary, the analytical approach tends to overestimate AC losses compared to the FEM model, particularly due to the sharper peaks in the analytical results. This leads to a more conservative estimation, which may be advantageous for conductor design by providing a safety margin in the thermal budget.

Another possible alternative for reducing losses is to striate the tape to create filaments. A recent study examined the effects of tape striation in TSTC [37]. The competing effects of stacking effect and striation combine in a complex manner to contribute to the AC losses, and in the high magnetic field limit, the losses in TSTC are efficiently reduced. Therefore, the use of striated tapes can also be considered a valid solution for loss mitigation in fusion cables operating in high-field conditions.

6. Conclusion

The magnetization losses of a new HTS sector-cable concept for fusion magnets have been investigated. Three possible layouts have been considered, differing in the number of tapes per stack or in the tape width, while maintaining the same amount of superconductor in the cable section. To evaluate instantaneous power losses during a high-field cycle, we developed a new analytical model that extends and combines the two original models by Bean–London and Brandt–Halse.

The new analytical model, which includes the field dependence of the critical current density, has been benchmarked against FEs simulations based on the T-A formulation. In addition, the analytical approach used in this study, despite its simplifications, provides a reliable and conservative estimation of AC losses in superconducting conductors. Although it assumes infinite dimensions and unidirectional current distribution, it offers a useful first-order approximation. This conservative nature is advantageous for conductor design, as it provides a safety margin in loss prediction when experimental data or full numerical simulations are not available.

Moreover, we found that the FE typically requires over 10 h of computation time on a machine equipped with a 3.70 GHz Intel Xeon processor, with 4 cores and 64 GB of RAM), while the analytical model provides results in just a few seconds. This efficiency highlights the analytical model's potential for applications requiring fast results, such as rapid prototyping. The analytical model could also be valuable in refining the FEM model, with a combined approach that may help improve both methods moving forward.

In conclusion, we have demonstrated that such analytical model is capable of reproducing the losses of a cable composed of stacks with a reduced number of tapes with sufficient accuracy. As known, the use of narrower tapes has a significant effect in reducing losses, and this is well described by our analytical formulation. Conversely, the division of stacks into sub-stacks has been shown to have a negligible effect.

However, in selecting the optimal layout, practical aspects such as industrial manufacturing must also be taken into consideration. For instance, the option with narrower tapes, having triple the number of stacks per sector, could potentially pose practical challenges in certain manufacturing steps. Therefore, a trade-off between design feasibility and loss optimization

still needs to be considered. Furthermore, the findings of this study also support the use of striated tapes once they are commercially available on a large scale.

Data availability statement

All data that support the findings of this study are included within the article (and any supplementary files).

Acknowledgments

This work has been carried out within the framework of the COST Action CA19108 'High-Temperature SuperConductivity for AcceLerating the Energy Transition' (Hi-SCALE), and the EUROfusion Consortium, funded by the European Union via the Euratom Research and Training Programme (Grant Agreement No 101052200 - EUROfusion). Views and opinions expressed are however those of the author(s) only and do not necessarily reflect those of the European Union or the European Commission. Neither the European Union nor the European Commission can be held responsible for them.

ORCID iDs

Gianluca De Marzi https://orcid.org/0000-0002-5752-2315
Luigi Muzzi https://orcid.org/0000-0001-8465-3364
Francesco Grilli https://orcid.org/0000-0003-0108-7235

References

[1] Whyte D G, Minervini J, LaBombard B, Marmar E, Bromberg L and Greenwald M 2016 Smaller & sooner: exploiting high magnetic fields from new superconductors for a more attractive fusion energy development path *J. Fusion Energy* **35** 41–53
[2] Sedlak K *et al* 2020 Advance in the conceptual design of the european demo magnet system *Supercond. Sci. Technol.* **33** 044013
[3] Heller R, Gade P V, Fietz W H, Vogel T and Weiss K-P 2016 Conceptual design improvement of a toroidal field coil for EU DEMO using high-temperature superconductors *IEEE Trans. Appl. Supercond.* **26** 1–5
[4] Corato V *et al* 2022 The demo magnet system - status and future challenges *Fusion Eng. Des.* **174** 112971
[5] Sarasola X, Wesche R, Ivashov I, Sedlak K, Uglietti D and Bruzzone P 2020 Progress in the design of a hybrid HTS-Nb_3Sn-Nb Ti central solenoid for the EU DEMO *IEEE Trans. Appl. Supercond.* **30** 1–5
[6] Giannini L, Boso D P and Corato V 2022 A combined electromagnetic and mechanical approach for EU-DEMO toroidal field coils *Appl. Sci.* **12** 2766
[7] Muzzi L *et al* 2023 Design and feasibility assessment of an hts sector shaped high-current conductor for fusion coils *IEEE Trans. Appl. Supercond.* **33** 1–6
[8] Zappatore A, De Marzi G and Uglietti D 2023 Impact of hysteresis losses in hybrid (HTS-LTS) coils for fusion applications *IEEE Access* **11** 100465–78
[9] De Marzi G and Corradini M 2021 High field-rate losses in cable-in-conduit-conductors carrying transport current *Presented at the 14th Chats on Applied Superconductivity (Chats-AS)* (Cadarache)
[10] Dutoit B, Grilli F and Sirois F 2023 *Numerical Modeling of Superconducting Applications* (World Scientific)
[11] Bean C P 1964 Magnetization of high-field superconductors *Rev. Mod. Phys.* **36** 31–39
[12] Kim Y B, Hempstead C F and Strnad A R 1962 Critical persistent currents in hard superconductors *Phys. Rev. Lett.* **9** 306–9
[13] Zhang X, Zhong Z, Ruiz H S, Geng J and Coombs T A 2016 General approach for the determination of the magneto-angular dependence of the critical current of ybco coated conductors *Supercond. Sci. Technol.* **30** 025010
[14] Blatter G, Feigel'man M V, Geshkenbein V B, Larkin A I and Vinokur V M 1994 Vortices in high-temperature superconductors *Rev. Mod. Phys.* **66** 1125–388
[15] Bai Song L 2024 private communication (Shanghai Superconductor Technology Co.)
[16] Civale L *et al* 2004 Understanding high critical currents in $YBa_2Cu_3O_7$ thin films and coated conductors *J. Low Temp. Phys.* **135** 87–98
[17] Tarantini C, Jaroszynski J, Kametani F, Zuev Y L, Gurevich A, Chen Y, Selvamanickam V, Larbalestier D C and Christen D K 2011 Anisotropy of the irreversibility field for zr-doped (y,gd)$Ba_2Cu_3O_{7-x}$ thin films up to 45 t *Phys. Rev.* B **84** 224514
[18] COMSOL Multiphysics® v. 6.2. 2020 COMSOL AB, Stockholm, Sweden (available at: www.comsol.com)
[19] Liang F, Venuturumilli S, Zhang H, Zhang M, Kvitkovic J, Pamidi S, Wang Y and Yuan W 2017 A finite element model for simulating second generation high temperature superconducting coils/stacks with large number of turns *J. Appl. Phys.* **122** 043903
[20] Zhang H, Zhang M and Yuan W 2016 An efficient 3D finite element method model based on the t-a formulation for superconducting coated conductors *Supercond. Sci. Technol.* **30** 024005
[21] Macchiagodena A, Breschi M, Buonafine D, De Marzi G and Savoldi L 2023 Analytical modeling of magnetization losses in twisted stacked hts conductors *IEEE Trans. Appl. Supercond.* **33** 1–5
[22] Mikitik G P, Mawatari Y, Wan A T S and Sirois F 2013 Analytical methods and formulas for modeling high temperature superconductors *IEEE Trans. Appl. Supercond.* **23** 8001920–8001920
[23] Halse M R 1970 AC face field losses in a type II superconductor *J. Phys. D: Appl. Phys.* **3** 717
[24] Brandt E H and Indenbom M 1993 Type-II-superconductor strip with current in a perpendicular magnetic field *Phys. Rev.* B **48** 12893–906
[25] London H 1963 Alternating current losses in superconductors of the second kind *Phys. Lett.* **6** 162–5
[26] Awaji S *et al* 2015 AC losses of an HTS insert in a 25-T cryogen-free superconducting magnet *IEEE Trans. Appl. Supercond.* **25** 1–5
[27] Kajikawa K, Awaji S and Watanabe K 2016 AC loss evaluation of an HTS insert for high field magnet cooled by cryocoolers *Cryogenics* **80** 215–20
[28] Brandt E H 1995 Electric field in superconductors with rectangular cross section *Phys. Rev.* B **52** 15442–57
[29] Mawatari Y 1996 Critical state of periodically arranged superconducting-strip lines in perpendicular fields *Phys. Rev.* B **54** 13215–21

[30] Grilli F, Ashworth S and Stavrev S 2006 Magnetization AC losses of stacks of YBCO coated conductors *Physica* C **434** 185–90
[31] Grilli F, Brambilla R and Martini L 2007 Modeling high-temperature superconducting tapes by means of edge finite elements *IEEE Trans. Appl. Supercond.* **17** 3155–8
[32] Gu F, Zhao Y, Zhong L, Duan X, Song M, Zhang B, Li Z and Hong Z 2019 Numerical study on magnetization losses in soldered-stacked-square (3S) HTS wires with 1 mm width *IEEE Trans. Appl. Supercond.* **29** 1–5
[33] Vargas-Llanos C R, Huber F, Riva N, Zhang M and Grilli F 2022 3D homogenization of the T-A formulation for the analysis of coils with complex geometries *Supercond. Sci. Technol.* **35** 124001
[34] Takayasu M, Chiesa L, Bromberg L and Minervini J V 2011 HTS twisted stacked-tape cable conductor *Supercond. Sci. Technol.* **25** 014011
[35] Campbell A 1982 A general treatment of losses in multifilamentary superconductors *Cryogenics* **22** 3–16
[36] Uglietti D, Kang R, Wesche R and Grilli F 2020 Non-twisted stacks of coated conductors for magnets: analysis of inductance and AC losses *Cryogenics* **110** 103118
[37] Lee M, Yoon M, Lee J-K, Park S, Choi K and Kim W-S 2024 Analysis of magnetization losses of twisted stacked-tape cables with striated strands *IEEE Trans. Appl. Supercond.* **34** 1–5